REPRINT

SPIE—The International Society for Optical Engineering

Reprinted from

Proceedings of

Lasers in Surgery: Advanced Characterization, Therapeutics, and Systems VI

27–30 January 1996
San Jose, California

SPIE P PROCEEDINGS SERIES

Volume 2671

Dynamic Simulations of Tissue Welding

Duncan J. Maitland, David C. Eder, Richard A.
London, Michael E. Glinsky, and Barbara A. Soltz‡

Lawrence Livermore National Laboratory, Livermore, CA 94550;
‡Conversion Energy Enterprises, Spring Valley, NY 10977

ABSTRACT

The exposure of human skin to near-infrared radiation is numerically simulated using coupled laser, thermal transport and mass transport numerical models. The computer model LATIS is applied in both one-dimensional and two-dimensional geometries. Zones within the skin model are comprised of a topical solder, epidermis, dermis, and fatty tissue. Each skin zone is assigned initial optical, thermal and water density properties consistent with values listed in the literature. The optical properties of each zone (*i.e.* scattering, absorption and anisotropy coefficients) are modeled as a kinetic function of the temperature. Finally, the water content in each zone is computed from water diffusion where water losses are accounted for by evaporative losses at the air-solder interface. The simulation results show that the inclusion of water transport and evaporative losses in the model are necessary to match experimental observations. Dynamic temperature and damage distributions are presented for the skin simulations.

2. INTRODUCTION

Laser-tissue welding is a time and temperature dependent process. Historically, the development of clinical energy delivery techniques have resulted in an empirical evolution of laser parameters, added chromophores, cooling water drips, and visual cues that meter delivery endpoints (see Bass and Treat[1]). More recently, investigators have utilized feedback control, including surface temperature[2] and reflectance[3], to quantify dynamic changes in relevant parameters. The goal of these control systems is to link the dynamic variable signatures to an optimum energy delivery. The limitation of these surface-based systems is that they don't provide information through the depth of the weld site. Hence, without additional information, the time-temperature history through the full thickness of the weld is unknown. This supplemental information is usually supplied via histologic assessment of the volumetric energy delivery. However, the use of histology in an iterative design process intended to optimize energy delivery is time consuming. We therefore turn to numerical modeling to quantify the volumetric energy-based changes that occur during the welding process. The goal of this effort is to demonstrate the model's capability to include all the physics relevant to laser-tissue energy delivery and subsequent tissue heating, desiccation, and damage.

In general, the three-dimensional, time-temperature history of tissue is described by a heat transfer equation (a.k.a. bioheat equation). Comprehensive references describing bioengineering heat transfer are readily available[4,5]. A variety of energy source and sink terms in the bioheat equation account for laser coupling, blood perfusion, etc. Here the bioheat equation is coupled with a Monte Carlo model of radiation transport in the LATIS (LAser -TISsue) computer program that has been previously described[6].

The commonly encountered versions of the bioheat equation, however, do not account for two important terms that are specific to water transport within and on the surface of heated tissue. First, surface evaporation of water may be a dominant energy term in the bioheat equation[7]. Secondly, as water is removed from the surface via evaporation, the water density gradient results in water diffusion through the porous tissue. As the water moves through the tissue, it carries its

0-8194-2045-X/96/$6.00

internal energy with it. Thus, the water-mass diffusion results in a convective energy term in the bioheat equation. Though not as dominant as the evaporation energy term, the mass diffusion still accounts for significant changes in the temperature history of the sub-surface tissue as well as predicting the desiccation of tissue, which in itself is significant.

3. MODELING

The computer program LATIS is applied in both one-dimensional (1-D) and two-dimensional (2-D) geometries. The exposure of human skin to near-infrared radiation is numerically simulated using coupled Monte Carlo, thermal transport and mass transport, models.

3.1 Sample geometry and properties

A generic model of skin is used to test the LATIS program. Figure 1. shows a schematic of the geometry used in the numerical simulations with the appropriate dimensions identified for each layer. The 1-D and 2-D configurations used throughout this report are described in Figure 1. The native properties for each model constituent are listed in Table 1. Dynamic variations of the native properties are described in the text below.

3.2 Light transport

Light transport is calculated with a Monte-Carlo method. Photons are followed time dependently. A fixed number of photons are introduced into the problem for each time-step. For most of the calculations in this study 200 photons/time step were used. Results changed insignificantly when 1000 photons were used. Scattering is calculated with a Henyey-Greenstein phase function. Absorption is calculated analytically. Each photon is assigned a weight which decreases with absorption. When a photon's weight drops below 1%, it is retired from the Monte-Carlo calculation. The absorbed energy is tabulated in spatial zones where it serves as a source term in the bioheat equation.

The non-linear coupling of the bioheat equation with the optical properties appears as a kinetic model that has been previously reported[6,15]. For example, the correlation between tissue damage (kinetics) and the dynamic changes in the scattering coefficient are given by

$$\mu_s(t,T) = \mu_s|_{native} \cdot f_{native} + \mu_s|_{denatured} \cdot f_{denatured}\ , \tag{1}$$

where f_{native} and $f_{denatured}$ are the concentration fractions of the two species in a binary kinetic system. Thus, $f_{native} + f_{denatured} = 1$. The fraction of native tissue molecules can be described by an exponential function of the Arrhenius damage integral

$$f_{native} = e^{-\int k\, dt}, \tag{2}$$

where the rate constant, k [s^{-1}], is described by

$$k = \frac{K_B\, T}{h}\, e^{\left[\frac{\Delta S}{R} - \frac{\Delta H}{RT}\right]}. \tag{3}$$

Here, K_B is Boltzman's constant, h is Planck's constant, R is the universal gas constant, T is the temperature (°K), and ΔS and ΔH are the entropy and enthalpy of the kinetic process, taken to be 0.824 kJ/mol-°K and 368 kJ/mol, respectively[16]. The model used a seven-fold increase in the scattering of skin tissue and the ICG solder in the denatured state. Dynamic changes in the absorption coefficient and anisotropy factor were not incorporated in the current simulations.

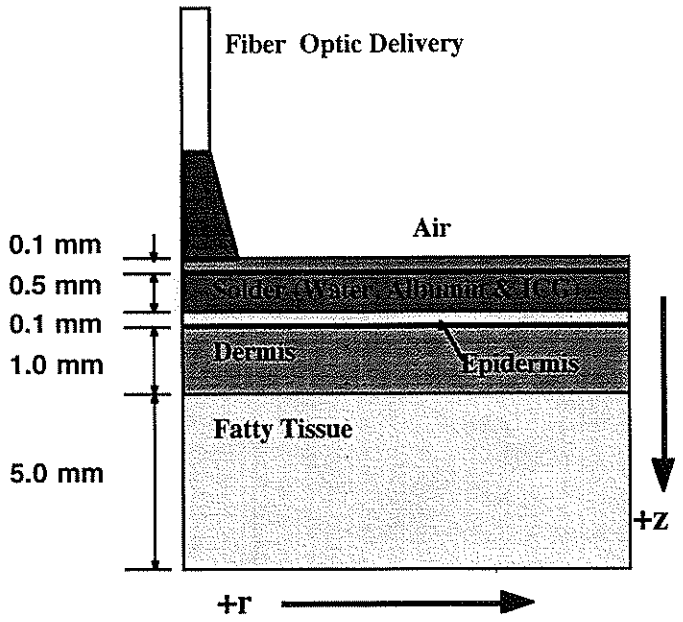

Figure 1. Schematic of laser irradiated skin. Cylindrical symmetry is utilized. The laser radiation is coupled into the tissue via a fiber, shown at the top. The diverging beam results in a certain fluence incident on the solder. Positive directions for the cylindrical coordinates z and r are shown. The solder is comprised of water, albumin and indocyanine green dye. The 2-D simulations use the geometry, except for the fiber delivery, as shown. The 1-D simulations are applied to the constituents aligned with the center of the incident spot, or the leftmost edge of the diagram.

Table 1. Summary of Optical and Thermal Parameters for Skin

Tissue/ Sample	Thermal, 1 atm, rm temp				Optical, 805 nm			
	% H_2O (weight)	ρ g/cm^3	K W/m^oK	c $J/g\text{-}^oK$	n -	g -	μ_s cm^{-1}	μ_a cm^{-1}
solder	74 [a]	1.12 [e]	0.44 [g]	3.48 [g]	1.37 [h]	0.80 [j]	10 [j]	10 [j]
epidermis	70 [b]	1.04 [f]	0.32 [g]	4.0 [f]	1.37 [h]	0.82 [i]	410 [i]	0.4 [i]
dermis	70 [c]	1.04 [f]	0.37 [f]	4.0 [f]	1.37 [h]	0.82 [i]	410 [i]	0.4 [i]
fatty tissue	20 [d]	0.85 [e]	0.16 [g]	2.07 [g]	1.37 [h]	0.80 [b]	100 [b]	0.5 [b]

[a] defined by solder composition
[b] estimated
[c] Jacques and Prahl[8]
[d] Spells[9]
[e] Cooper and Trezek[10]
[f] Diller[11]
[g] Welch[12]
[h] Bolin *et. al.*[13]
[i] van Gemert *et. al.*[14]
[j] Glinsky *et. al.*[15]

3.3 Thermal transport

The bioheat equation is given by

$$c\rho\frac{\partial}{\partial t}[T(r,t)] = \nabla K \nabla[T(r,t)] + Q_{source} + Q_{evaporation} + Q_{water\ diffusion}. \tag{4}$$

Values for heat capacity, c, density, ρ, and thermal conductivity, K, are listed in Table 1 for standard conditions. The source term is the energy coupled from the light transport, which is described in section 3.2. The evaporation and water diffusion terms are described below. Radiative and blood perfusion losses were ignored.

3.4 Evaporation

The $Q_{evaporation}$ term of equation 4 can be estimated by computing

$$Q_{evaporation} = \frac{\dot{n}_{H_2O}\,\Delta H_{vaporization}}{\Delta x}, \tag{5}$$

where $\dot{n}_{H_2O}$ is the mass flux of water vapor away from the water surface [g/(m^{2}s)], $\Delta H_{vaporization}$ is the temperature dependent latent heat of vaporization of water [J/g], and Δx is the water layer thickness over which the evaporation occurs [m]. The latent heat is a nonlinear function of temperature. A polynomial fit to tabulated data[17] for the latent heat of vaporization was used over the 0-200 °C temperature range.

An expression for the mass flux per unit area in equation 5 is[18]:

$$\dot{n}_{H_2O} = \frac{D_{H_2O} M_{H_2O}}{R}\frac{\partial}{\partial x}\left[\frac{P_{H_2O}}{T_{H_2O}}\right], \tag{6}$$

where D_{H_2O} is the water vapor diffusion coefficient through air [m^2/s]; M_{H_2O} is the molecular weight of water, 18, [g/mol]; R is the universal gas constant, 8.31, [J/mol °K]; P_{H_2O} is the vapor pressure of the water [Pa]; T_{H_2O} is the temperature of the water vapor [°K]; and $\frac{\partial}{\partial x}$ is the vapor gradient [1/m]. Equation 6 describes the water vapor diffusion that occurs due to a water vapor gradient. That is, the high concentration of water vapor near the solder surface diffuses toward the dry air some distance away from the water surface. The use of the evaporation term in the bioheat equation is dependent on an assumption that the boundary layer is a steady-state condition. This implies that the there is laminar air flow parallel to the air-tissue interface. The steady-state mass boundary condition leads to approximate analytic expressions for all the parameters in equation 6 that are a function of the boundary layer (D_{H_2O}, P_{H_2O}, T_{H_2O}, $\frac{\partial}{\partial x}$). A linear approximation of D_{H_2O} is obtained by calculating the average of the temperature-dependent diffusion coefficient at the solder surface and at the top edge of the boundary layer. Using an empirical formula for the temperature dependence of D_{H_2O}[18], the linear approximation is given by

$$\overline{D}_{H_2O} = 0.13\left[1+\left(\frac{T_{solder\,surface}}{T_{air}}\right)^{\frac{3}{2}}\right]. \tag{7}$$

The vapor pressure and temperature differential is approximated as

$$\partial\left[\frac{P_{H_2O}(T_{H_2O})}{T_{H_2O}}\right] = \left.\frac{P(T)}{T}\right|_{\text{solder surface}} - \left.\frac{P(T)}{T}\right|_{\text{air}} x H_{\text{relative}} \quad (8)$$

where the vapor pressures are computed as saturated pressures at the given boundary layer edge and $H_{relative}$ is the relative humidity far away from the tissue surface. The vapor pressure at the solder surface is assumed equal to the saturated pressure. The saturated vapor pressure has an exponential temperature dependence. A polynomial fit of water data for temperatures in the range 0-100 °C was used in the calculations[17].

For our problem, the boundary layer defines the distance over which a water vapor density gradient occurs. In general, however, the boundary layer is defined by the flow velocity, u, parallel to the solder surface (laminar flow). The flow gradient results in a water vapor density (and temperature) gradient that is used as the boundary condition for the evaporation term. We have assumed that a steady-state air flow exists such that a steady-state boundary condition exists for the mass transfer. The simulations used a boundary layer thickness of 0.39 cm (∂x), which corresponds to an air velocity of 1 cm/s.

3.5 Water Diffusion

Evaporation of water from the tissue surface produces a gradient that causes the sub-surface water to diffuse toward the tissue surface. The diffusion of liquid water through the porous tissue is described by Fick's law[19]:

$$\frac{\partial}{\partial t}\rho_{H_2O} = \nabla\rho\ D\nabla\left[\frac{\rho_{H_2O}}{\rho}\right], \quad (9)$$

where ρ is the total density, ρ_{H_2O} is the water density, and D is the diffusion coefficient for water through dermis (D_{dermis} = $5x10^{-6}$ cm^2/s)[20]. The diffusion coefficient was assumed constant though all layers of the skin.

As the surface of the tissue is desiccated, the diffusion of sub-surface water toward the surface results in a convective energy term in equation 4:

$$Q_{\text{water diffusion}} = \rho_{H_2O}\ c\ u_{\text{diffusion}} \bullet \nabla T, \quad (10)$$

where $u_{diffusion}$ is the time-dependent diffusion velocity that results from equation 9.

4. RESULTS

Figure 2 shows the influence of evaporation on tissue temperature distributions. The 1-D simulations show that, given the same incident laser fluence on the same tissue, the evaporative cooling limits the solder surface temperature below 100 °C. Further, the tissue temperatures never exceed 80 °C; which is in stark contrast to the no evaporation case where tissue temperatures remain well above 100 °C 60 seconds after the laser has been turned off.

The desiccation of the near-surface tissue is shown in Figure 3. The water diffusion model first demonstrates the desiccation of the sub-surface tissues as the solder layer is depleted by evaporation, which occurs as long as the surface temperature is sufficiently elevated. After the laser is turned off, Figure 3 shows that the water content of the epidermis starts to increase as water from deep in the tissue diffuses toward the surface. As the water diffuses from the cooler depths toward the hotter surface, the diffusion results in a net decrease in the tissue temperatures. The addition of the water mass diffusion

to the evaporative losses results in an average 4 °C decrease through the full thickness skin temperatures over the latter 60 seconds, after the laser had been turned off (data not shown in figures).

An example of a 2-D simulation is shown in Figure 4. Contour plots of the temperature are shown in Figures 4(a)-(c) at 30, 60 and 90 seconds, respectively. The geometry and parameters used in this simulation are described in Figure 1, Table 1 and section 3 of this report. The laser energy was turned off after the first 60 seconds. The cumulative damage, which is defined by the equation 2, is shown in Figure 4(d) at a time of 120 seconds. The results show that at least 63% of the tissue was denatured through the full thickness of the 1.0 mm-thick dermis in the center of the laser spot.

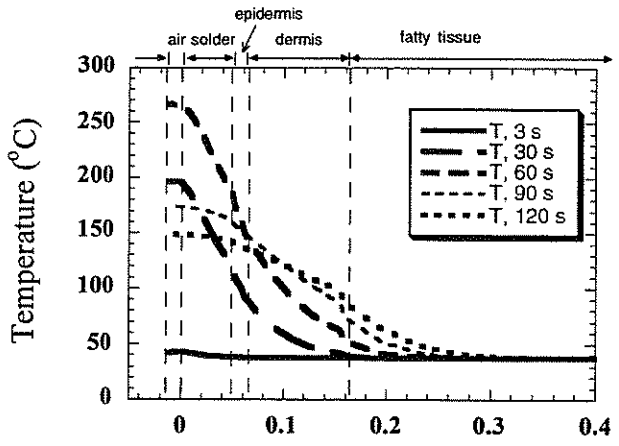

(a)

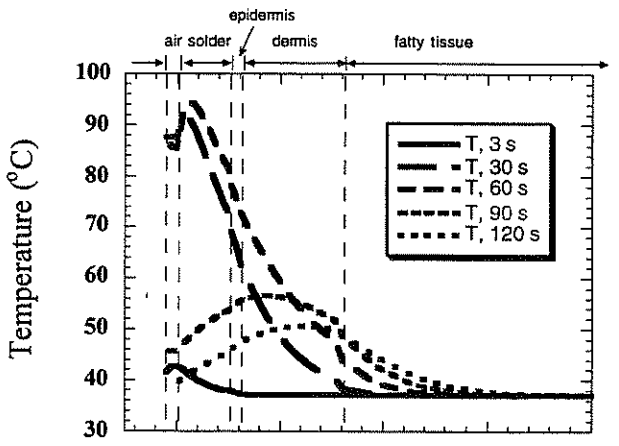

(b)

Figure 2. The effect of evaporation on skin temperatures. Figures (a) and (b) show the temperature as a function of depth for the same 1-D skin parameters and the same fluence rate (4 W/cm^2). Each figure shows temporal snap-shots of the tissue temperature for times between 3 and 120 seconds. The laser energy was turned on between 0-60 seconds. Without evaporation, Figure 2 (a) shows that the solder-surface temperature would rise above 200 °C with dermis temperatures reaching 150 °C. With evaporative cooling turned on, Figure 2 (b) shows that the solder surface temperature never reaches 100 °C and tissue temperatures fall below 50 °C in 120 s.

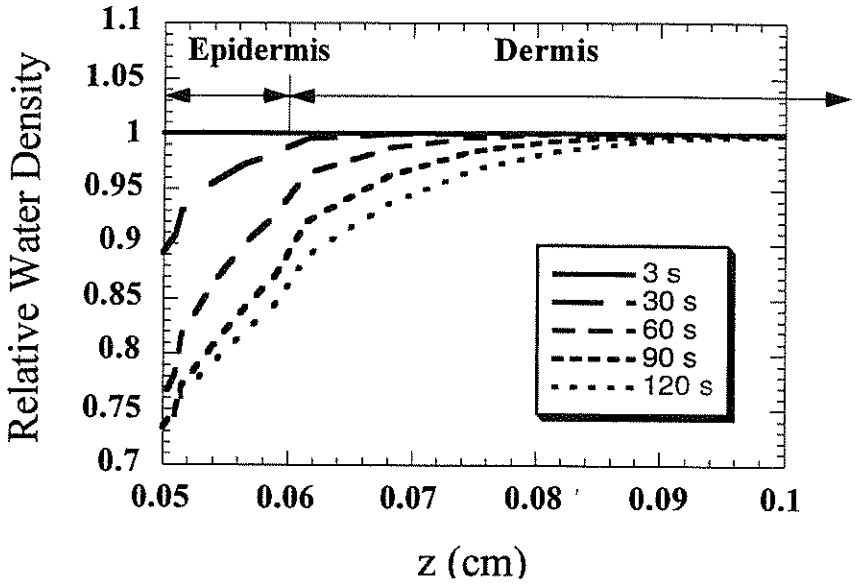

Figure 3. Desiccation of the skin. The progressive desiccation of the epidermis during irradiation is shown. The laser energy was turned on between 0-60 seconds.

5. DISCUSSION

The results show that the inclusion of water transport is important for accurately simulating the time-dependent temperature distributions in laser-irradiated skin. The numerical program, LATIS, includes the dynamic coupling between radiation transport, thermal transport and mass transport models. Here, we have added and tested the mass transport coupling to the bioheat equation with evaporative boundary conditions. Without evaporation, the model produces unrealistically high temperature distributions that contradict our experimental observations[21]. With evaporation, LATIS predicts temperature distributions that qualitatively agree with our observations that surface temperatures do not vary far from 100 °C. In the future, we shall perform quantitative comparisons of the simulations and experiments.

LATIS is a tool that will help assess the three-dimensional dynamics of tissue welding environments. As was demonstrated in this investigation, LATIS is capable of simulating the laser-tissue interactions of heterogeneous tissues with two-dimensional symmetry and non-linear coupling between radiation, thermal transport, and mass diffusion models. Thus, as empirical relations between welding mechanisms and dynamically measurable variables are found, LATIS provides the ability to monitor these reactions in a two-dimensional geometry. The tissue damage results in Figure 4(a) is an example of an empirical, in this case kinetic, predictive capability. The influence of pulsed laser systems, laser spot size and geometry variations are other examples of LATIS's predictive capabilities. Further, with the modification of our current models, LATIS will serve as a design tool in investigating signatures or dynamic changes in observable parameters like reflectance or birefringence.

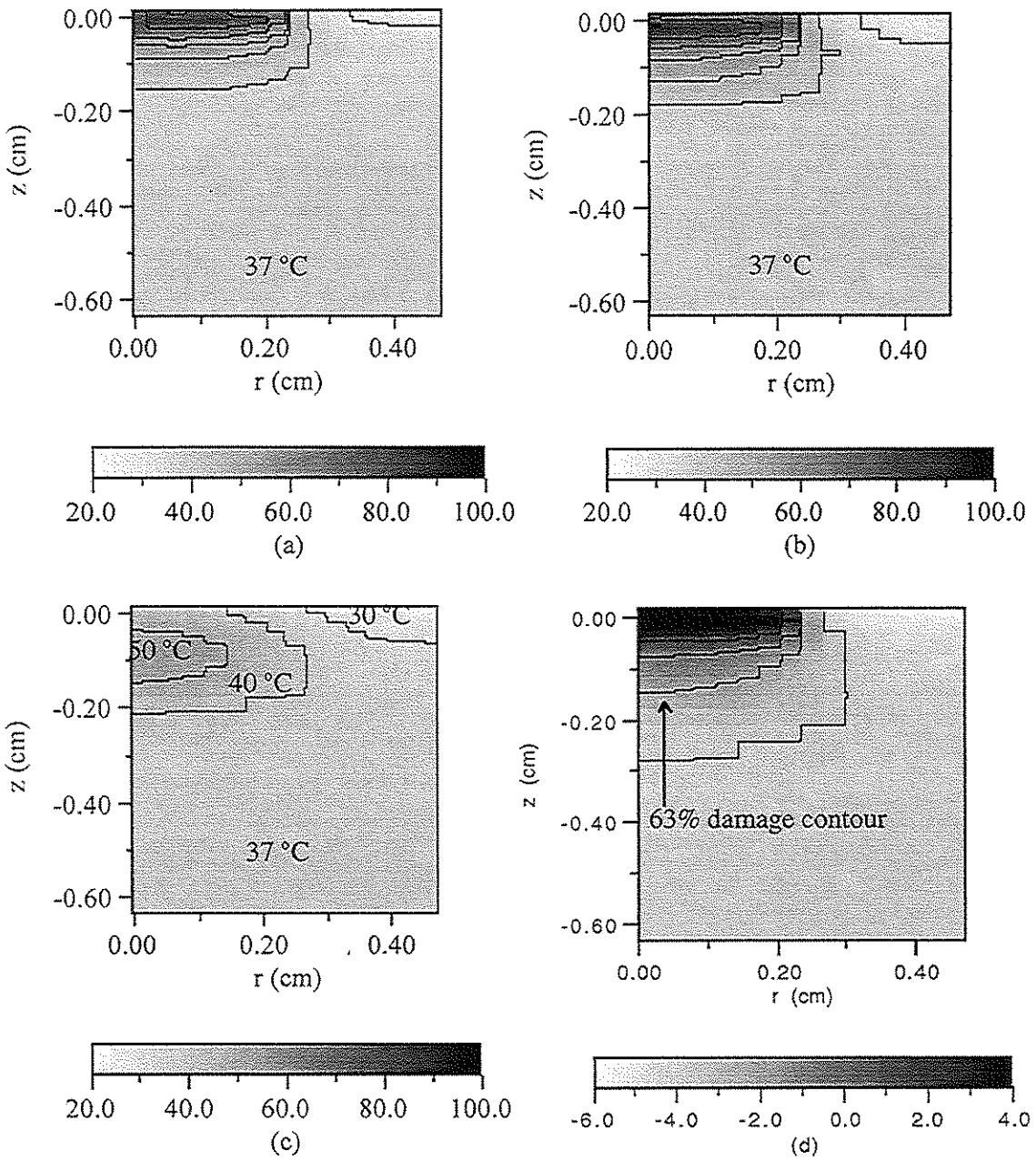

Figure 4. Temperature history of laser irradiated skin. The 2-D geometry in these figures is depicted in Figure 1. Figures (a) - (c) show the temperature distributions at 30, 60 and 90 seconds, respectively, in skin when irradiated with a 4 W/cm^2, 0.5 cm spot size laser for 60 seconds. Temperatures are in degrees Celsius. The contour lines occur at 10 °C intervals. Figure (d) shows the accumulated damage of the skin after 120 seconds. The grayscale of figure (d) is a logarithmic plot of the Arrhenius damage integral shown in the exponent of equation 2. The value of 0.0 indicates that 63% of the tissue defined by this contour has been denatured.

6. ACKNOWLEDGMENTS

This work was performed under the auspices of the US. Department of Energy by the Lawrence Livermore National Laboratory under Contract W-7405-ENG-48. The authors wish to thank W. Small IV, N. Heredia and P. Celliers for helpful discussions. Also, the authors wish to thank L. Bass for providing the solder recipe.

7. REFERENCES

1. Bass, L.S. and M.R. Treat, "Laser tissue welding: A comprehensive review of current and future clinical applications," Lasers Surg. Med. **17**, 315-349, 1995.
2. Stewart, R.B., A. Benbrahim, G.M. LaMuraglia, M. Rosenburg, G.J. L'Italien, W.M. Abbot, and R.T.V. Kung, "Laser assisted vascular welding with real time temperature control," *Lasers Surg. Med.*, in press.
3. Chamberraz, F., K. Schonenberger, G. Delacretaz, R.P. Salathe, G. Godlewski, J. Tang and M. Prudhomme, "Laser tissue welding : A new device controlled by reflectance," *Medical Applications of Lasers II*, Proceedings SPIE, **2327**, 172-180, 1994.
4. Welch A.J., and M.J.C. van Gemert, eds., *Optical-Thermal Response of Laser-Irradiated Tissue*, New York, NY: Plenum Press, 1995.
5. Cho, Y.I., ed., *Advances in Heat Transfer*, San Diego, CA: Academic Press, 1992.
6. London R.A., M.E. Glinskey, G.B. Zimmerman, D.C. Eder and S.L. Jacques, "Coupled light transport-heat diffusion model for laser dosimetry with dynamic optical properties", Laser-Tissue Interaction VI, Proceedings SPIE, **2391**, 434-442, 1995.
7. Torres, J.H., M. Motamedi, J.A. Pearce and A.J. Welch, "Experimental evaluation of mathematical models for predicting the thermal response of tissue to laser irradiation," *Appl. Opt.* **32**, 597-606, 1993.
8. Jacques, S.L. and S.A. Prahl, "Modeling optical and thermal distributions in tissue during laser irradiation," *Lasers Surg. Med.* **6**, 494-503, 1987.
9. Spells, K.E., "The thermal conductivities of some biological fluids," *Phys. Med. Biology* **5**, 139-153, 1960.
10. Cooper, T.E. and G.J. Trezek, "Correlation of thermal properties of some human tissue with water content," *Aerosp. Med.:* **42**, 24-27, 1971.
11. Diller, K.R., "Modeling of bioheat transfer processes," in *Advances in Heat Transfer*, Y.I. Cho Ed. Boston: Academic Press, 157-347, 1992.
12. Welch, A.J., "The thermal response of laser irradiated tissue," *IEEE J. of Q.E.* **QE-20**, 1471-1481, 1984.
13. Bolin, F.P., L.E. Preuss, R.C. Taylor, and R.J. Ference, "Refractive index of some mammalian tissues using a fiber optic cladding method," *Appl. Opt.* **28**, 2297-2303, 1989.
14. van Gemert, M.J.C., Jacques, S.L., Sterenborg, H.J.C.M., and Star, W.M., "Skin optics," *IEEE Trans. Biomed. Eng.* **36**, 1146-1154, 1989.
15. Glinsky, M.E., R.A. London, G.B. Zimmerman and S.L. Jacques, "Modeling of endovasculature patch welding using the computer program LATIS," in *Laser-Tissue Interaction V I*, Proc. SPIE Vol. **2391**, p. 262, 1995.
16. Maitland, D.J. and J.T. Walsh, Jr., "Quantitative measurements of linear birefringence during the heating of native collagen," accepted in *Lasers Surg. Med.* , November, 1994.
17. Lide, D.R., Editor-in-Chief, *Handbook of Chemistry and Physics*, 74th Edition, Boca Raton: CRC Press 1993, p. 6-10.
18. Hisatake, K.,S. Tanaka and Y. Aizawa, "Evaporation rate of water in a vessel," *J. Appl. Phys.* **73**, pp. 7395-7401, 1993.
19. Welty, J.R., C.E. Wicks and R.E. Wilson, *Fundamentals of Momentum, Heat, and Mass Transfer*, 3rd Ed., John Wiley & Sons, 1984.
20. Scheuplein, R.J. and I.H. Blank, "Permeability of the skin," *Physiol. Rev.* **51**, 702-747, 1971.
21. Small, W., IV, N.J. Heredia, P.M. Celliers, L.B. Da Silva, D.C. Eder, M.E. Glinsky, R.A. London, D.J. Maitland, and B.A. Soltz, "Laser tissue welding mediated with a protein solder," in *Laser Welding: Control, Delivery Systems, and Clinical Applications*, SPIE Proceedings, Vol. **2671**, 1996.